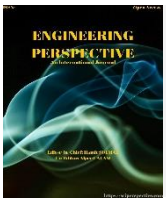

e-ISSN:2757-9077

ENGINEERING PERSPECTIVE

https://sciperspective.com/ Research Paper

# Design and Optimisation of a Double Wishbone Independent Suspension System for an L6 Electric Vehicle: A Response Surface Methodology Based Design Application

Mohammad Nassar [1], Kübra Polat[1*], Yağmur Koçlu[1], Mehmet Murat Topaç[1]

[1] *Mechanical Engineering Department, Faculty of Engineering, Dokuz Eylül University, İzmir, 35397, Turkey*

ABSTRACT

Suspensions are vital vehicle subsystems that provide ride comfort, stability and handling while absorbing shocks caused by road irregularities. Their designs require careful consideration of structural integrity, weight reduction and performance optimisation. In light electric vehicles, such as those in the L6 class, the design and optimisation of suspension systems becomes even more critical due to design compactness and functionality. The aim of this study is to design a front independent suspension system for an electric L6 class vehicle and to outline an optimisation-based design process of this design by Finite Element Analysis (FEA). In the first stage of the study, various load cases and the effects of these loads on the connection points were determined and force analyses were performed. Then, a preliminary design was built to withstand the types of loading to which it will be subjected. Afterwards, FEA was performed on the preliminary design using the data obtained from the force analysis. As a result of this analysis, critical load case and critical regions were identified. In the optimisation stage, the outer diameter (D), wall thickness (t) and radius of curvature (R) were defined as input parameters, while mass, equivalent stress and total deformation were selected as output parameters. As a result of the optimisation-based design, a stress reduction of approximately 43% was observed at the critical region. In addition, the percentage of the influence was investigated in order to better understand the effects of the basic design parameters. Among the parameters, the wall thickness was found to be the design parameter which has the highest effect on stress distribution and part mass.

**Keywords:** Electric vehicles; Electromobility; Design optimisation; Independent suspension; Vehicle component design

**History**
Received: 28.10.2024
Accepted: 15.01.2025

**Author Contacts**
**Corresponding Author*
e-mail addresses : k.polat@ogr.deu.edu.tr

**How to cite this paper:** Nassar, M., Polat, K., Koçlu, Y., Topaç, M.M., (2025). Design and Optimisation of a Double Wishbone Independent Suspension System for an L6 electric Vehicle: A Response Surface Methodology Based Design Application. Engineering Perspective, 5 (1), 21-30. http://dx.doi.org/10.29228/eng.pers.79569

## 1. Introduction

The global population is increasing by 240,000 people per day and 90 million people per year, leading to an increasing demand for vehicles [1]. As technology continues to improve, mobility demand is projected to grow three times faster than population growth [2]. This increase in the number of vehicles contributes significantly to air pollution, which increases exhaust emissions and poses serious risks to public health. In many countries, the automotive sector is responsible for 48% of the total carbon dioxide ($CO_2$) emissions [3]. Furthermore, modern cities are facing a traffic crisis, leading to more noise and traffic congestion. The energy crisis, which is worsening due to decreasing fossil fuel resources, is becoming more serious over time [4]. The European Commission's Roadmap to a Single European Transport Area Towards aims to reduce traffic and pollution problems as one of its objectives towards a competitive and clean transport system [5]. In order to achieve this goal, vehicle manufacturers have had to realise a series of improvements in order to adapt to competitive conditions. There is also a need to provide safer and more economical options to effectively address environmental and population issues. As a result, the use of light electric vehicles is growing rapidly. Many cities have started to use light vehicles for urban transport. This plays an important role in solving various problems, especially in the freight transport sector [6].

The lower centre of gravity of electric vehicles makes their suspension design extremely important for traction and stability. Small electric vehicles, especially those classified in the L6 category, are increasingly incorporating independent suspension systems in their design to improve ride quality and handling. There are also different types of suspension systems for such vehicles in the literature [6]. Independent suspension is a widely used system in automotive engineering, characterised by the ability of each wheel to move vertically independently of the other; this design feature is essential in improving the overall stability and dynamic behaviour of the vehicle, contributing to handling and ride comfort.

The double wishbone suspension system is essentially considered to be a four-bar mechanism; one side is connected to the chassis, considered to be the ground, and the other side is connected to the wheel via a steering knuckle [7]. The double wishbone suspension system has several advantages over other suspension systems.

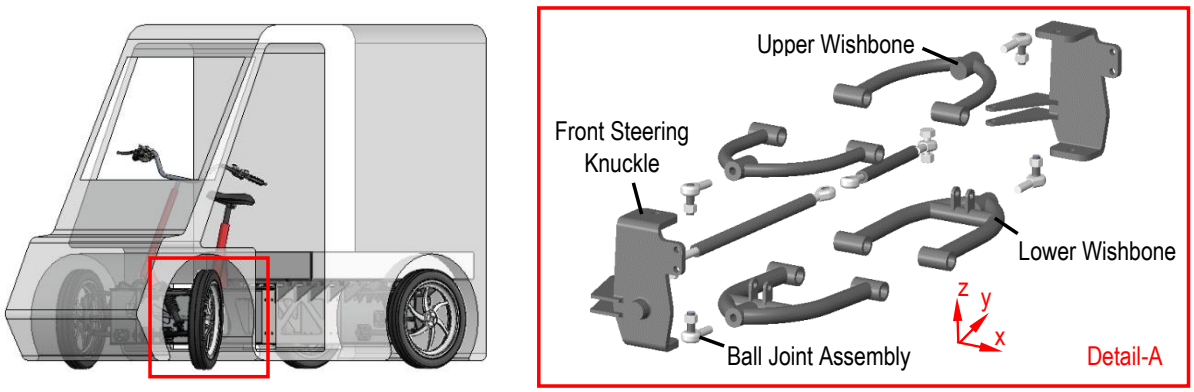


a b

Figure 1. Suspension system components and their integration in the vehicle

Due to its many design parameters, it is more flexible and versatile, allowing the kinematics of the vehicle to be controlled and adapted to specific applications. It can also reduce the weight of the unsprung mass, improving the vehicle's dynamic characteristics, although it is more complex to design than other suspension systems [8]. There are several methods in the literature for designing and analysing double wishbone suspension systems for light electric vehicles. The double wishbone suspension system consists of an upper wishbone, lower wishbone, shock absorber, steering system and steering knuckle as shown in Figure 1.

The shock absorber is mounted on the upper or lower arm and is responsible for absorbing road inputs to provide ride comfort. The wishbone holding the shock absorber carries/bears more load, so it is called the carrier wishbone, while the other wishbone is called the control wishbone [9]. Double wishbone suspension system is also called short-long suspension system, with the upper arm being the shorter arm and the lower arm the longer arm [7]. In general, when designing wishbones, it is important to provide a difference in length between the control and carrier arms as they affect the wheel angle change, camber change and to some extent the track width change during the vertical movement of the wheel. Reducing the length of the control arm will result in a positive camber in rebound and a negative angle when compressed, which is desirable when designing a suspension system [10].

Response Surface Methodology (RSM) is widely used in various industries, one of the most important of which is the automotive industry [11-13]. RSM is a method used to determine the effect of independent variables in a system on dependent parameters. This approach allows for efficient design modifications and ensures that structural rigidity is maintained. In a study using ANSYS® Workbench, a mass reduction analysis of a motor mounting bracket was performed using RSM method and a mass reduction of 4.31% was achieved by keeping the failure load constant [14]. In another study, the crash analysis of the bumper beam and energy absorber was carried out and then the RSM method was used for the optimal design [15]. A RS-based design of a multi-link steering mechanism is carried out to reduce the deviation in toe angle duo to wheel travel and optimum steering error during the steering angle range [16].

In a study focusing on the design of a lightweight solar-powered vehicle suspension, a double wishbone suspension system was designed and Finite Element Analysis (FEA) was performed to investigate the differences between Macpherson and double wishbone suspension systems via static analysis [17]. In another study, ANSYS® Workbench was used for steering knuckle design and topology optimisation to reduce unspring mass [18]. Furthermore, kinematic analysis was performed on double wishbone suspension to determine camber and toe changes depending on kingpin using analytical methods [19]. Moreover, a half-car model with five Degrees of Freedom (DoF) was designed in another study where a vibration model for an electric mini off-road vehicle was built using MATLAB® software to investigate the frequency response and optimise ride comfort [20].

In this study, the design and optimisation of a front independent suspension for an L6e vehicle is carried out. Firstly, a joint force analysis was performed to determine the forces acting on the hardpoints of the system. Then, a parametric modelling process was carried out using SOLIDWORKS® software. FEA was performed on the lower wishbone under specified load conditions using ANSYS® Workbench. Design of Experiments (DoE) - Response Surface (RS) optimisation methods were used to find the optimum design in terms of weight and stress. Finally, in order to check the

safety of the obtained optimal geometry under operating conditions, an assembly model was created and a FEA was performed on this model again.

The design parameters that should be taken into consideration in front independent suspension design have been determined. The effects of these design parameters on component performance were also analysed in this study, and it is aimed to guide the designer. In general, the component design steps are summarised.

To the best of the authors' knowledge, there is no study in the open literature that provides a roadmap for the mechanical design of the suspension elements used in this class of vehicles. This study aims to fill this lack to some extent.

## 2. Material and method

### 2.1 Method

In this research, DoE and RS methods are employed to determine the optimum design of the system by modifying desired parameters within specified ranges and constraints. DoE is the examination of the system during processing by applying several tests and changing input parameters to study the system's response [21]. RS is also carried out, which involves using mathematical equations to develop and optimize the system, especially considering various parameters that affect system performance [22]. In this study, DoE and RS are performed using the ANSYS® Workbench response surface optimization tool. For a second-order response surface model, the model is defined as [23]:

$$y = \beta_0 + \sum_{i=1}^{k} \beta_i x_i + \sum_{i \le j}^{k} \beta_{ij} x_i x_j + \varepsilon \quad (1)$$

This model can also be expressed as a matrix.

$$y = X\beta + \varepsilon \quad (2)$$

Here, y is the vector of observations, X is the model matrix, β is the vector which includes the intercept parameter $\beta_0$ and the partial regression coefficients, and ε is the vector of random errors that directly affect β [21].

Central Composite Design (CCD), a method for determining optimal parameter values, is used in this study, which is available as an option in the DoE module's design table definition. This method is commonly used in the DoE studies. The main objective of CCD is to determine the effects of factors affecting a system and the optimum levels of these factors. It provides a design structure that evaluates the linear, quadratic and interactional effects of these factors. [21,22,24]. The advantages of CCD include the ability to estimate the dependent variables nonlinearity, efficiently obtain maximum information with minimum experimental data, and reduce the number of experiments required to estimate the quadratic terms in a quadratic model [25]. It is widely used for solving complex multifactorial problems. With its capability to develop accurate and reliable second-order regression models, CCD provides a deeper understanding of data and enables meaningful explanation [26]. The summary scheme of the optimisation study is summarised in Figure 2.

## 3. Design Steps

### 3.1 Load model

In the analyses performed within the scope of this study, the loads acting on the suspension system specified in the literature were used for FEA in the stress state evaluation and optimisation process of the mechanical design. In addition to the vertical load, driving, braking and lateral forces acting on a vehicle wheel in the most general driving condition [7]. These loads are shown in Figure 3 as vertical load P, side load S and braking or driving load B. These load combinations on the suspension system are applied to the wheel contact point shown as R [27]. In the literature, there are 16 main load conditions for the suspension system [28]. Bumping, brake-in- turn and cornering load conditions are considered as critical scenarios of the suspension system.

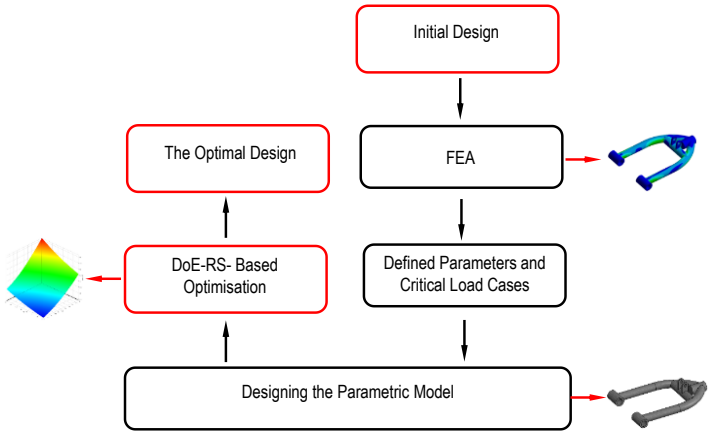


Figure 2. Summary structural optimization process of the lower wishbone

### 3.2. Joint Forces

FEA was performed to determine the reaction loads acting on the suspension system joints. The joint loads for three different load cases were calculated using the vector analysis. The forces applied to the contact area of the wheel are resisted and carried by the spring, control or carrier wishbones, and the steering knuckle on the load condition.

The joint forces are calculated according to the hardpoints of the suspension. The hardpoints of the system are evaluated by considering two main factors. The first one is that the instantaneous centre of the suspension arms should be near the ground to reduce the effect of camber and track width variation. Another critical factor is the distance between the centre of mass and the instantaneous centre. This distance is of crucial importance for the roll dynamics of the vehicle, especially in roll angle calculations [27,29]. Since gravity and suspension component self-weights are negligible compared to the vehicle loads, these effects are neglected in the calculations. The free body diagram of the main components of the suspension system is presented in Figure 4. Equivalent forces and moments were applied to each body within the framework of the action response principle in accordance with [29]. According to force balance:

$$\{F_{D43}\} = -\{F_{D34}\} \quad (3)$$

$$\{F_{G42}\} = -\{F_{G24}\} \quad (4)$$

$$\{F_{H45}\} = -\{F_{H54}\} \quad (5)$$

$$\{F_{C37}\} = -\{F_{C73}\} \quad (6)$$

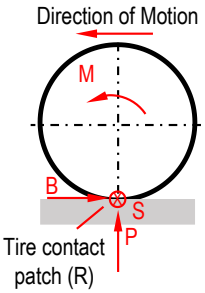


| | P | S | B |
|---|---|---|---|
| Bumping | 2 g | 0 | 0 |
| Cornering | 1 g | 1.25 g | 0 |
| Brake-in-Turn | 1 g | 0.75 g | 0.75 g |

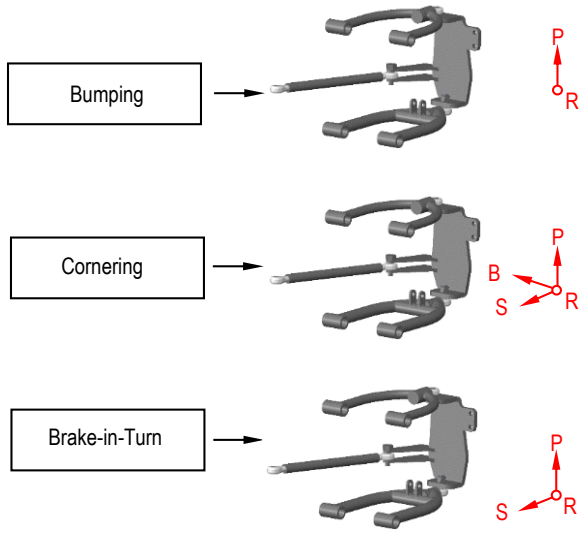


Figure 3. Critical load cases acting on the suspension system

The equivalent forces (F) and moment (M) from the lower wishbone free body diagram:

$$\sum \{F_2\} = \{0\} \quad (7)$$

$$\{F2\} = \begin{bmatrix} FFx \\ FEx \\ FGx \end{bmatrix} + \begin{bmatrix} FFy \\ FEy \\ FGy \end{bmatrix} + \begin{bmatrix} FFz \\ FEz \\ FGz \end{bmatrix} = \begin{bmatrix} 0 \\ 0 \\ 0 \end{bmatrix} \quad (8)$$

$$\sum \{F_2\} = \{0\} \quad (9)$$

$$\sum \{M_{G2}\} = \{0\} \quad (10)$$

$$\sum \{M_{G2}\} = \{RFG\}x\{F2\} + \{REG\}x\{FE\} \quad (11)$$

$$\{RFG\} = \begin{bmatrix} 0 & -RFGz & RFGy \\ RFGz & 0 & -RFGx \\ -RFGy & RFGx & 0 \end{bmatrix} \quad (12)$$

$$\{REG\} = \begin{bmatrix} 0 & -REGz & REGy \\ REGz & 0 & -REGx \\ -REGy & REGx & 0 \end{bmatrix} \quad (13)$$

The above calculations were also performed for the other bodies of the suspension. When the general calculations of the whole system are analysed, it is seen that there are 18 equations and 20 unknowns in total. Two equations are defined for the connections between the upper and lower wishbones and the chassis. In addition, it is possible to write the following two equations in accordance with [29].

$$\{FF\} \cdot \{REF\} = \{0\} \quad (14)$$

$$\{FB\} \cdot \{RAB\} = \{0\} \quad (15)$$

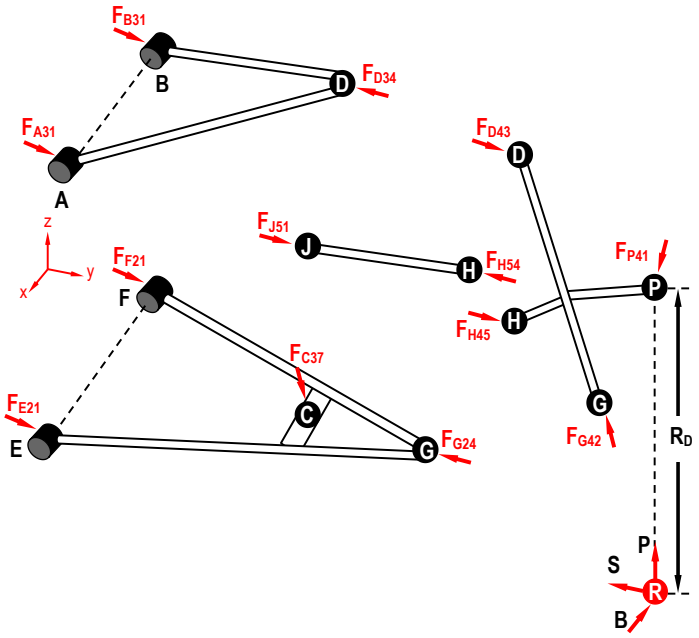


Figure 4. Free body diagram and reaction joint forces

Finally, a 19 x 19 matrix was formed as shown in Figure 5. By taking the inverse of this matrix and multiplying it with the load matrix, the equations of the free body diagram were solved [29].

The changes in the x, y and z components of the reaction forces of the carrier arm and control arm are shown in Figure 6. In the lateral load condition, it is observed that the lower wishbone spherical joint is subjected to approximately twice as much load as the upper spherical joint. In the vertical load scenario, it was found that most of the applied force was carried by the lower wishbone.

### 3.3 Design criteria of the lower wishbone

For the initial design of the lower wishbone, the structure was assumed as a beam. The cross-sectional dimensions were determined by elementary stress analysis. The lower wishbone is subjected to bending by the vertical component of the spring force and shearing due to the braking force. Additionally, the horizontal component of the spring force applies a compressive load on the lower wishbone. The calculations were carried out according to the condition where the spring force at the spring connection point shown as C reaches

its maximum value. With these calculations, the initial design was built by determining the value for both the outer radius (D) and the inner radius (d), which ensures the safety and durability of the lower wishbone. The initial configuration shown in Figure 7.

These bending and shear stresses are calculated by the following equations:

$$\sigma_{Bending}=\frac{M_{max}\times D}{2*I} \quad (16)$$

$$W=\pi\frac{D^4-d^4}{64} \quad (17)$$

$$\sigma_{Normal}=\frac{Fc_y}{A} \quad (18)$$

$$\sigma_B+\sigma_N<\sigma_{Safety} \quad (19)$$

In the brake-in-turn case, the stress concentration on the welding joint is critical due to the shear normal and bending loads. The forces acting on the system were taken from the analytical joint matrix given in Figure 5 and applied to the lower wishbone arm to determine the minimum thickness of the weld joint radius.

For safety reasons, the lower wishbone arm is assumed as a cantilever beam. Weld thickness value represented by “a” in Figure 8 is calculated. The safety factor used in the whole system was determined as 1.6. The normal, shear and bending stress equations:

$$\sigma_N=\frac{F}{A}=\frac{F_{Cy}-F_{Gy}}{\pi\frac{((R+2a)^2-R^2)}{4}} \quad (20)$$

$$\tau_S=\frac{F}{A}=\frac{F_{Gz}-F_{Cz}}{\pi\frac{((R+2a)^2-R^2)}{4}} \quad (21)$$

$$\tau_B=\frac{M}{W}=\frac{F_{Gz}*Lg-F_{Cz}*Lc}{\pi\frac{((R+2a)^3-R^3)}{32}} \quad (22)$$

$$\sigma_c=\sqrt{\sigma^2+\Sigma\tau^2}\leq\sigma_{yield}* \text{ Factor of Safety} \quad (23)$$

| | | | | | | | | | | | | | | | | | | | |
|---|---|---|---|---|---|---|---|---|---|---|---|---|---|---|---|---|---|---|---|
| 1 | 0 | 0 | 1 | 0 | 0 | 0 | 0 | 0 | 0 | 0 | 0 | 0 | 0 | 0 | 0 | 0 | 0 | fcx | -FGx |
| 0 | 1 | 0 | 0 | 1 | 0 | 0 | 0 | 0 | 0 | 0 | 0 | 0 | 0 | 0 | 0 | 0 | 0 | fcy | -FGy |
| 0 | 0 | 1 | 0 | 0 | 1 | 0 | 0 | 0 | 0 | 0 | 0 | 0 | 0 | 0 | 0 | 0 | 0 | fcz | -FGz |
| 0 | 0 | 0 | 0 | -RCGy | RCGz | 0 | 0 | 0 | 0 | 0 | 0 | 0 | 0 | 0 | 0 | 0 | 0 | (RhG*fc)x | -FDx |
| 0 | 0 | 0 | RCGx | 0 | -RCGz | 0 | 0 | 0 | 0 | 0 | 0 | 0 | 0 | 0 | 0 | 0 | 0 | (RhG*fc)y | -FDy |
| 0 | 0 | 0 | -RCGx | RCGy | 0 | 0 | 0 | 0 | 0 | 0 | 0 | 0 | 0 | 0 | 0 | 0 | 0 | (RhG*fc)z | -FDz |
| -1 | 0 | 0 | 0 | 0 | 0 | 0 | 0 | 1 | 0 | 0 | 0 | 0 | 0 | 0 | 0 | 0 | 0 | 0 | FFy |
| 0 | -1 | 0 | 0 | 0 | 0 | 1 | 0 | 0 | 1 | 0 | 0 | 0 | 0 | 0 | 0 | 0 | 0 | 0 | FFz |
| 0 | 0 | -1 | 0 | 0 | 0 | 0 | 1 | 0 | 0 | 1 | 0 | 0 | 0 | 0 | 0 | 0 | 0 | 0 | FEx |
| 0 | 0 | 0 | 0 | 0 | 0 | -RFGy | RFGz | 0 | -REGy | REGz | 0 | 0 | 0 | 0 | 0 | 0 | 0 | 0 | FEy |
| 0 | 0 | 0 | 0 | 0 | 0 | 0 | -RFGz | REGx | 0 | -REGz | 0 | 0 | 0 | 0 | 0 | 0 | 0 | 0 | FEz |
| 0 | 0 | 0 | 0 | 0 | 0 | RFGy | 0 | -REGx | REGy | 0 | 0 | 0 | 0 | 0 | 0 | 0 | 0 | 0 | FBx |
| 0 | 0 | 0 | -1 | 0 | 0 | 0 | 0 | 0 | 0 | 0 | 1 | 0 | 0 | 1 | 0 | 0 | fHx | 0 | FBy |
| 0 | 0 | 0 | 0 | -1 | 0 | 0 | 0 | 0 | 0 | 0 | 0 | 1 | 0 | 0 | 1 | 0 | fHy | 0 | FBz |
| 0 | 0 | 0 | 0 | 0 | -1 | 0 | 0 | 0 | 0 | 0 | 0 | 0 | 1 | 0 | 0 | 1 | fHz | 0 | FAx |
| 0 | 0 | 0 | 0 | 0 | 0 | 0 | 0 | 0 | 0 | 0 | 0 | -RBDy | RBDz | 0 | -RADy | RADz | MHDx | 0 | FAy |
| 0 | 0 | 0 | 0 | 0 | 0 | 0 | 0 | 0 | 0 | 0 | RBDx | 0 | -RBDz | RADx | 0 | -RADz | MHDy | 0 | FAz |
| 0 | 0 | 0 | 0 | 0 | 0 | 0 | 0 | 0 | 0 | 0 | -RBDx | RBDy | 0 | -RADx | RADy | 0 | MHDz | 0 | FC |
| 0 | 0 | 0 | 0 | 0 | 0 | 0 | 0 | 0 | 0 | 0 | RBAx | RBAy | RBAz | 0 | 0 | 0 | 0 | 0 | FH |

Figure 5. Reaction joint force matrix

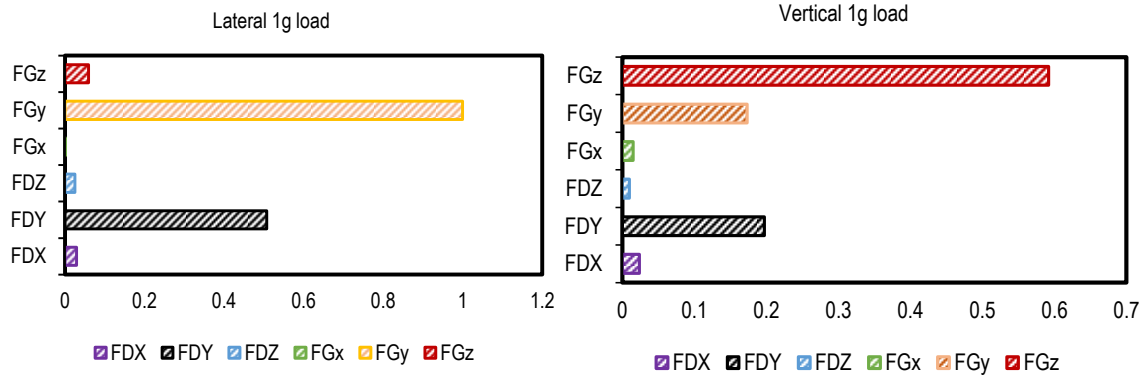


Figure 6. Reaction joint forces for load cases

In the brake-in-turn case, the stress concentration on the welding joint is critical due to the shear normal and bending loads. The forces acting on the system were taken from the analytical joint matrix given in Figure 5 and applied to the lower wishbone arm to determine the minimum thickness of the weld joint radius.

For safety reasons, the lower wishbone arm is assumed as a cantilever beam. Weld thickness value represented by “a” in Figure 8 is calculated. The safety factor used in the whole system was determined as 1.6. The normal, shear and bending stress equations:

$$\sigma_N=\frac{F}{A}=\frac{F_{Cy}-F_{Gy}}{\pi\frac{((R+2a)^2-R^2)}{4}} \quad (20)$$

$$\tau_S=\frac{F}{A}=\frac{F_{Gz}-F_{Cz}}{\pi\frac{((R+2a)^2-R^2)}{4}} \quad (21)$$

$$\tau_B = \frac{M}{W} = \frac{F_{Gz}*Lg - F_{Cz}*Lc}{\frac{\pi((R+2a)^3 - R^3)}{32}} \quad (22)$$

$$\sigma_c = \sqrt{\sigma^2 + \Sigma\tau^2} \leq \sigma_{yield} * \text{Factor of Safety} \quad (23)$$

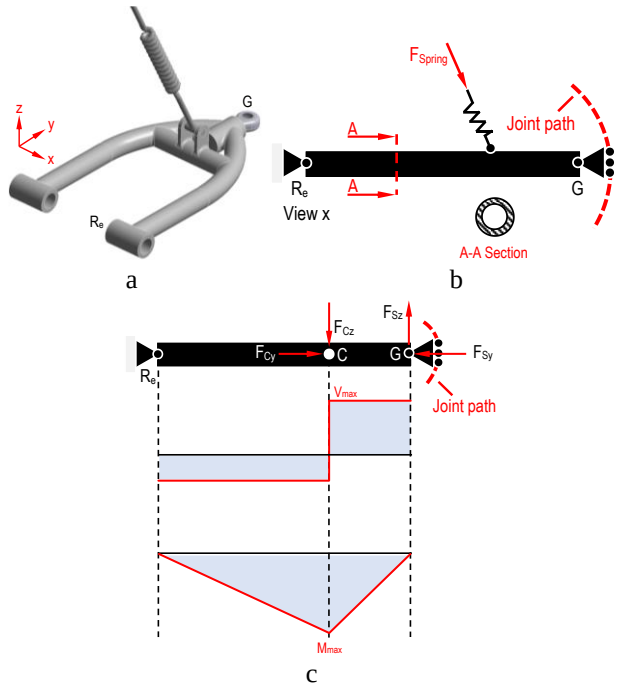


Figure 7. Load model of the lower wishbone

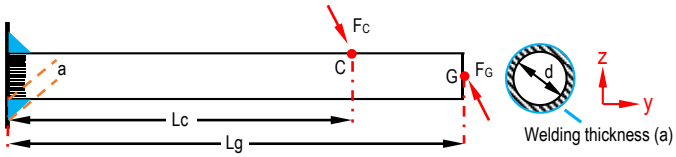


Figure 8. Defining the welding thickness of the lower wishbone arm

## 4. FEA model of the suspension system

The CAD model built parametrically in SOLIDWORKS® was transferred to ANSYS® Workbench for FEA. In the suspension system, the lower wishbone is considered as a critical component since the vertical force due to the vehicle weight is transferred from the spring to the lower wishbone. In the FEA model, a mesh structure consisting of 441,031 nodes and 254,729 elements was created using the SOLID187 element consisting of ten nodes. The mesh structure is shown in Figure 9. Some of the structural elements utilised in the analysis have been simplified due to the confidentiality policy of the project partner company.

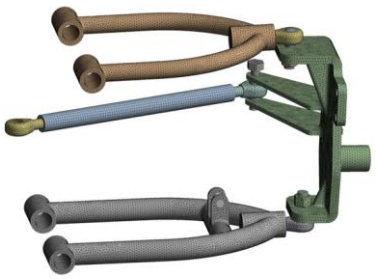

Figure 9. The mesh structure of FEA model

Firstly, in order to determine the stress conditions of the lower wishbone, two FEA models, a single component and a quarter vehicle, were built. The single component model is fixed through the wishbone bushings and the force is applied through the spherical and the spring joint of the lower arm. Then, to verify the stress values obtained from the single-component analysis, a quarter vehicle analysis was carried out by adding a revolute joint to the wishbone bushings, a ball joint to the knuckle linkages and a spring element. The spring is modelled with a pin joint in the bushing to transfer its force to the lower wishbone. In this analysis, the force was applied at the wheel contact point (R). The analysis models are given in Figure 10. Here, Fixed Joint "F", Revolute Joint (Ground) "$R_e$", Spherical Joint "S", Spherical Joint (Ground) "$S_e$", Contact Patch "R" and Dynamic Radius of the Tire "$R_d$" are named.

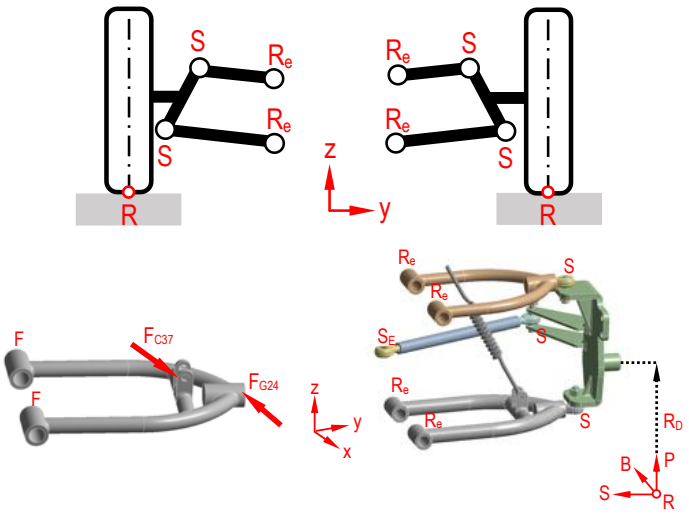


Figure 10. Boundary conditions used in FEA models

## 5. Result and Discussion

### 5.1 Critical load cases

The FEA of the quarter vehicle model was performed for three different load cases: bumping, cornering and brake-in-turn. In the analyses results shown in Figure 11, the stress values obtained are represented as the ratio of the maximum equivalent stress values occurring in the critical stress concentration regions. The brake-in-turn load condition was identified as the critical load case because of the braking force in addition to the spring load that supports and transmits the vehicle weight.

### 5.2 DoE based optimisation

The DoE-RS module of ANSYS® Workbench was used to determine the optimal arm design that is lightweight and at the same time stress safe. Firstly, the critical region was determined according to the FEA result. In this region, it was determined that both the stress value is maximum and it is subjected to tensile stress as shown in Figure 12.

Then, a parametric model of the initial design was built using SolidWorks®. For the DoE-based optimisation, the outer diameter (D), wall thickness (t) and tube curvature radius (R) were selected as design parameters as shown in Figure 13.

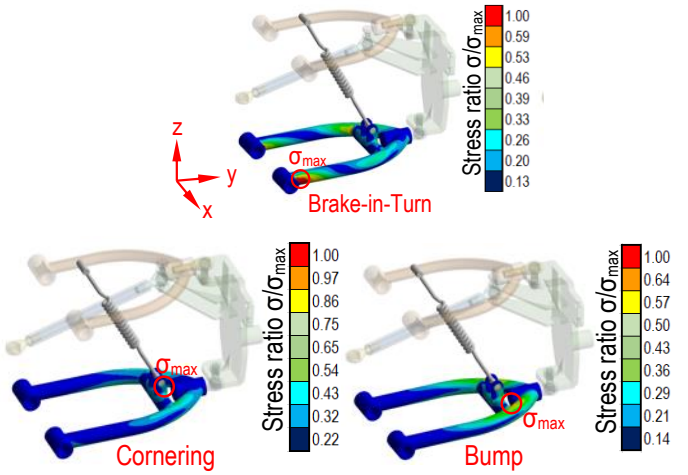


Figure 11. FEA of the lower wishbone for the load cases in quarter vehicle model

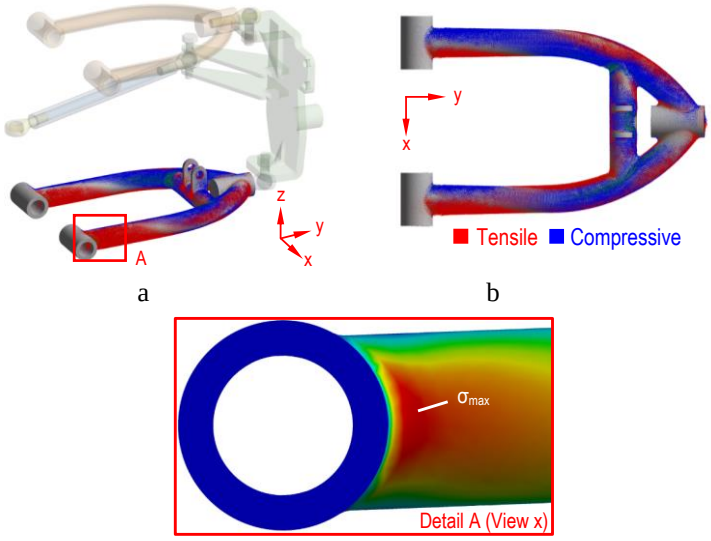


Figure 12.a and b. principal stress of the lower wishbone, c. the critical area

The current state of all parameters is considered as a unit and the maximum and minimum values are shown in Table 1 as multiples of this value in accordance with the confidentiality policy of the company. Mass, maximum equivalent stress and total deformation were defined as output parameters. As a result of the DoE performed over the critical load condition, RS graphs were obtained with these parameters.

Figure 14 shows the effect of the design parameters on the output values. When the graph is analysed, it was seen that the outer diameter (D) has the greatest effect especially on the maximum equivalent stress. As the diameter increases, the structural strength increases while the total deformation decreases. Thickness (t) was found to have the most sensitive effect on weight. Increasing the thickness significantly increases the mass but has a minimal effect on the equivalent stress. The curvature radius (R) has similar effects on both mass and maximum equivalent stress, but its effect on deformation is more pronounced. Increasing the curvature radius may affect the elastic behaviour of the structure, making it more sensitive to deformation.

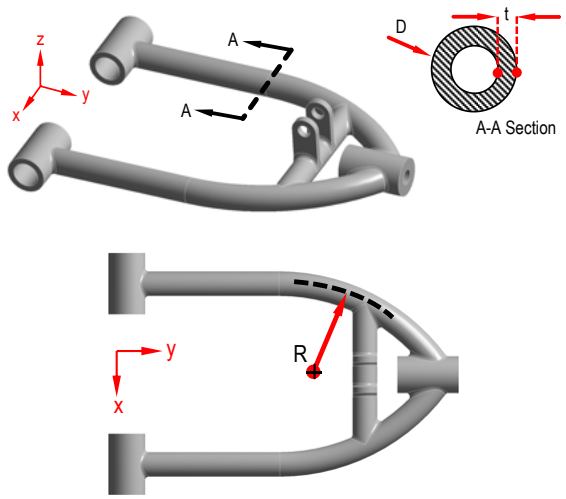


Figure 13. The design parameters of the lower wishbone arm

Table1. Parameters variation range

| Parameters | Variation Range |
|---|---|
| t | 1.5t < t < 2.2t |
| D | 20D < D < 25D |
| R | 130R < R < 165R |

As a result, ensuring the equilibrium between design parameters is critical to achieve the desired performance. For example, while the outer diameter can be increased to minimise deformation, this must be balanced with weight optimisation.

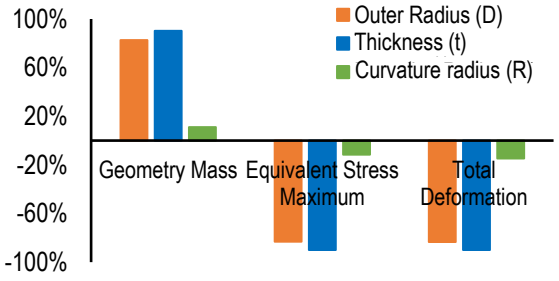


Figure 14. Effective percentage of the design parameters effecting the lower wishbone

The RS plots generated for mass, equivalent stress and total deformation using the defined input parameters are shown in Figure 15. These graphs provided the optimum design points to be determined in the optimisation module. In the optimisation process, minimising the equivalent stress and mass was determined as the main design objective.

A final design was created by using the values obtained as a result of the optimisation. FEA was applied to this final model again. Six points ($P_1$-$P_6$) were randomly selected from this region in order to examine the stress variation in the critical region. The stress change between the initial design and the final design is shown in Figure 16. In this graph, point $P_6$ of the final design is selected as reference.

Other point's stresses were calculated by ratio to the stress at this point. When the graph is examined, it was observed that the stress values of the final design were lower than the initial design at all points. The percentage decrease values from $P_1$ to $P_6$ were determined as 42.94%, 33.75%, 26.92%, 32.01%, 41.32% and 40.31%, respectively.

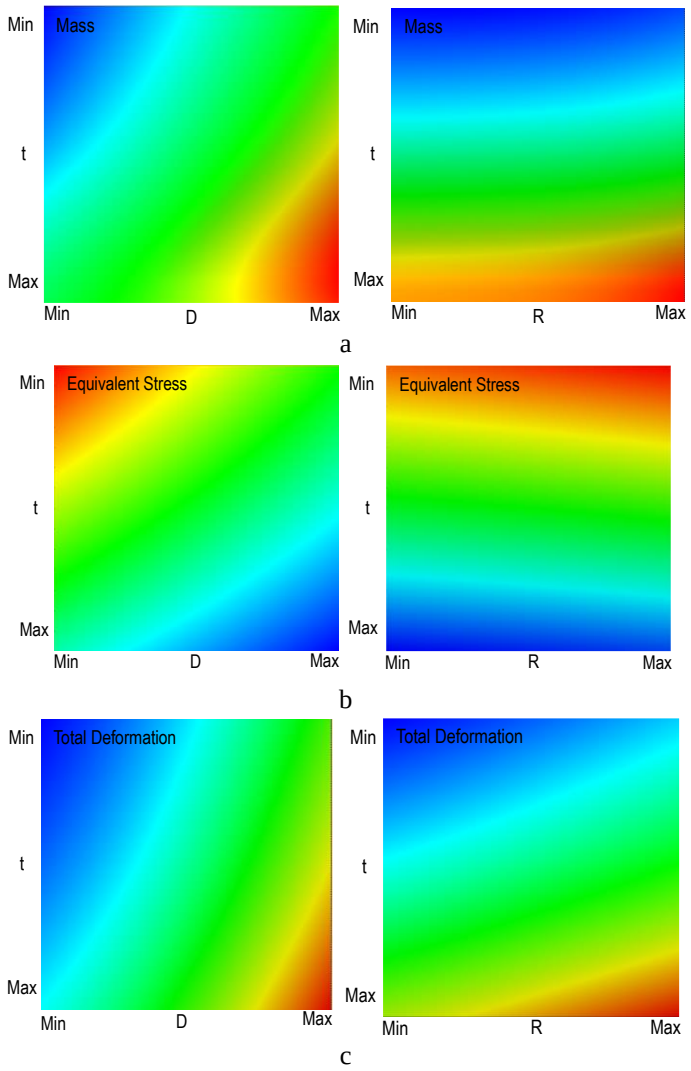


Figure 15. Response surfaces of the parameters, a- mass (kg), b- Equivalent Stress (MPa), c- Total Deformation (mm)

A final design was created by using the values obtained as a result of the optimisation. FEA was applied to this final model again. Six points ($P_1$-$P_6$) were randomly selected from this region in order to examine the stress variation in the critical region. The stress change between the initial design and the final design is shown in Figure 16. In this graph, point $P_6$ of the final design is selected as reference. Other point's stresses were calculated by ratio to the stress at this point. When the graph is examined, it was observed that the stress values of the final design were lower than the initial design at all points. The percentage decrease values from $P_1$ to $P_6$ were determined as 42.94%, 33.75%, 26.92%, 32.01%, 41.32% and 40.31%, respectively.

The analysis results of the quarter vehicle model and the single component- based analysis model built with the final design are compared. According to Figure 17, the maximum stress values were represented as a percentage and an error rate of approximately 2.27% was determined. In addition, the critical zone identified as Region A in the quarter vehicle model analysis was found to match the critical Region B in the component-based analysis.

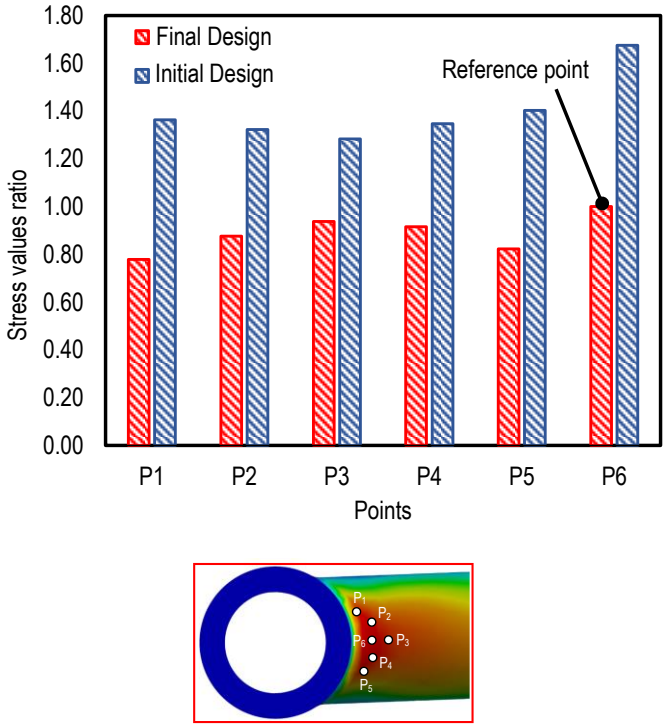


Figure 16. Response surfaces of the parameters, a- mass (kg), b- Equivalent Stress (MPa), c- Total Deformation (mm)

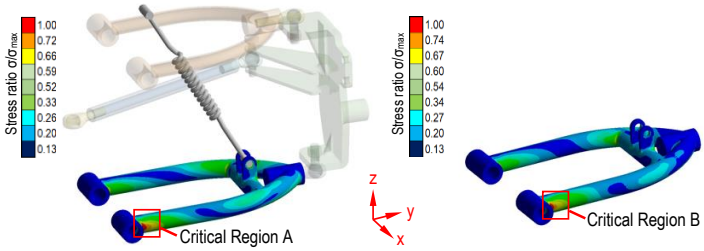


Figure 17. Comparison of the optimization singular and quarter vehicle model

## 6. Conclusion

In this study, the design, analysis and optimisation of the front independent suspension system of an electric L6 class vehicle were investigated. Firstly, different load cases and their effects at the joint points are analysed. Then, two models were built for FEA to be performed in ANSYS® Workbench using SOLIDWORKS® software. As a result of the FEA, the critical load model was identified. Also, the region subjected to both tensile and maximum stress was defined as the critical region. In the optimisation stage, the outer diameter (D), wall thickness (t) and radius of curvature radius (R) were selected as input parameters, while mass, equivalent stress and total deformation were chosen as output parameters. For optimal values, low mass and low stress design constraints were defined for the software and new parameter values were obtained for the final design.

Among these points, the highest stress reduction was obtained at point $P_1$ with approximately 43%. The results of the study also highlight the critical design parameters that should be taken into account in the design of independent suspension for electric L6 vehicles. The effects of these design parameters on the output parameters are also analysed. Thickness was found to have the highest effect on all output parameters. This study provides guidelines for the design of suspension systems for similar class vehicles.

## Conflict of Interest Statement

The authors must that there is no conflict of interest in the study.

## Acknowledgment

This study was supported by TÜBİTAK (The Scientific and Technological Research Council of Türkiye) within the framework of 2209-B program. The Authors acknowledge the technical support of Mr. Decan Alpargun, the founder of AZR Engineering. The authors also acknowledge Mr. Sefa Temur for the contribution to Figure 1.

## CRediT Author Statement

**Mohammad Nassar:** Data curation, Formal analysis, Software, Writing - original draft, **Kübra Polat:** Software, Writing - review & editing, Visualization, **Yağmur Koçlu:** Solid Modelling, Data curation, **Mehmet Murat Topaç:** Conceptualization, Supervision, Writing - review & editing

## References

1. Shaw, R. P. (1992). The impact of population growth on environment: The debate heats up. Environmental Impact Assessment Review, 12(1-2), 11-36.
2. Schafer, A. (1998). The global demand for motorized mobility. Transportation Research Part A: Policy and Practice, 32(6), 455-477.
3. Teixeira, A. C. R., da Silva, D. L., Machado Neto, L. D. V. B., Diniz, A. S. A. C., & Sodré, J. R. (2015). A review on electric vehicles and their interaction with smart grids: the case of Brazil. Clean Technologies and Environmental Policy, 17, 841-857. https://doi.org/10.1007/s10098-014-0865-x
4. Borowski, P. F. (2022). Mitigating climate change and the development of green energy versus a return to fossil fuels due to the energy crisis in 2022. Energies, 15(24), 9289. https://doi.org/10.3390/en15249289
5. European Commission. (2011). A roadmap for moving to a competitive low carbon economy in 2050 (COM/2011/144 final). European Union. Retrieved April 3, 2024, from https://eur-lex.europa.eu/LexUriServ/LexUriServ.do?uri=COM:2011:0144:FIN:EN:PDF
6. Ewert, A., Schmid, S., Brost, M., Davies, H., & Vinckx, L. (2021). Small electric vehicles: An international view on light three- and four-wheelers (p. 189). Springer Nature. https://doi.org/10.1007/978-3-030-65843-4
7. Jazar, R. N. (2008). Vehicle dynamics (Vol. 1). Springer.
8. Sancibrian, R., Garcia, P., Viadero, F., Fernandez, A., & De-Juan, A. (2010). Kinematic design of double-wishbone suspension systems using a multiobjective optimisation approach. Vehicle System Dynamics, 48(7), 793–813. https://doi.org/10.1080/00423110903156574
9. Littman, M. L. (1996, April). Simulations combining evolution and learning. In Santa Fe Institute Studies in the Sciences of Complexity-Proceedings Volume (Vol. 26, pp. 465–478). Addison-Wesley Publishing Co.
10. Reimpell, J., Stoll, H., & Betzler, J. (2001). The automotive chassis: Engineering principles. Elsevier.
11. Mahla, S. K., Safieddin Ardebili, S. M., Mostafaei, M., Dhir, A., Goga, G., & Chauhan, B. S. (2024). Multi-objective optimization of performance and emissions characteristics of a variable compression ratio diesel engine running with biogas-diesel fuel using response surface techniques. Energy Sources, Part A: Recovery, Utilization, and Environmental Effects, 46(1), 15737–15754. https://doi.org/10.1080/15567036.2020.1813847
12. Ardebili, S. M. S., Calam, A., Solmaz, H., Böğrek, A., & Haşimoğlu, C. (2024). Improving the combustion process of a homogeneous charge compression ignition engine running with triple fuel blend using response surface methodology. Journal of the Brazilian Society of Mechanical Sciences and Engineering, 46(8), 486. https://doi.org/10.1007/s40430-024-05060-0
13. Kocakulak, T., Arslan, T. A., Şahin, F., Solmaz, H., Ardebili, S. M. S., & Calam, A. (2023). Determination of optimum operating parameters of MWCNT-doped ethanol fueled HCCI engine for emission reduction. Science of The Total Environment, 895, 165196. https://doi.org/10.1016/j.scitotenv.2023.165196
14. Bildirici, D., Topaç, M. M., Polat, K., Zavrak, T., & Arman, Y. (2024). Failure analysis-based mass reduction of an aluminium alloy engine mounting bracket using Design of Experiments approach. Engineering Failure Analysis, 166, 108927. https://doi.org/10.1016/j.engfailanal.2024.108927
15. Yildirim, A., Demirci, E., Karagöz, S., Özcan, Ş., & Yildiz, A. R. (2023). Experimental and numerical investigation of crashworthiness performance for optimal automobile structures using response surface methodology and oppositional based learning differential evolution algorithm. Materials Testing, 65(3), 346–363. https://doi.org/10.1515/mt-2022-0304
16. Topaç, M. M., Deryal, U., Bahar, E., & Yavuz, G. (2015). Optimal kinematic design of a multi-link steering system for a bus independent suspension: An application of response surface methodology. Mechanics, 21(5), 404–413. https://doi.org/10.5755/j01.mech.21.5.11964
17. Odabaşı, V., Maglio, S., Martini, A., & Sorrentino, S. (2019). Static stress analysis of suspension systems for a solar-powered car. FME Transactions, 47(1), 70–76. https://doi.org/10.5937/fmet1901070o
18. Li, J., Tan, J., & Dong, J. (2020). Lightweight design of front suspension upright of electric formula car based on topology optimization method. World Electric Vehicle Journal, 11(1), 15. https://doi.org/10.3390/wevj11010015
19. Tanik, E., & Parlaktaş, V. (2015). Design of a very light L7e electric vehicle prototype. International Journal of Automotive Technology, 16, 997–1005. https://doi.org/10.1007/s12239-015-0102-6
20. Yu, B., Wang, Z., Zhu, D., Wang, G., Xu, D., & Zhao, J. (2020). Optimization and testing of suspension system of electric mini off-road vehicles. Science Progress, 103(1), 0036850419881872. https://doi.org/10.1177/0036850419881872
21. Montgomery, D. C. (2000). Design and analysis of experiments (5th ed.). John Wiley & Sons.
22. Myers, R. H., Montgomery, D. C., & Anderson-Cook, C. M. (2009). Response surface methodology: Process and product optimization using design of experiments (3rd ed.). John Wiley & Sons.

23. Han, H., & Park, T. (2004). Robust optimal design of multi-body systems. Multibody System Dynamics, 11, 167–183. https://doi.org/10.1023/B:MUBO.0000025414.28789.34
24. Aydın, M., & Ünlüsoy, Y. S. (2012). Optimization of suspension parameters to improve impact harshness of road vehicles. International Journal of Advanced Manufacturing Technology, 60, 743–754. https://doi.org/10.1007/s00170-011-3589-7
25. Rodriguez, R., Mazza, G., Zalazar-García, D., Fernandez, A., & Fabani, M. P. (2023). Polyphenol extraction from bio-wastes: Optimization and kinetic analysis. Studies in Natural Products Chemistry, 79, 317–339. https://doi.org/10.1016/B978-0-443-18961-6.00010-X
26. Gregor, M., Grznar, P., Mozol, S., & Mozolova, L. (2023). Design of simulation experiments using Central Composite Design. Acta Simulatio, 9(2). https://doi.org/10.22306/asim.v9i2.99
27. Topaç, M. M., Olguner, C., & Bahar, E. (2022). Development of an independent front suspension for truck tractors. Mechanics, 28(2), 121–129. https://doi.org/10.5755/j02.mech.29092
28. Heißing, B., Ersoy, M., & Gies, S. (Eds.). (2011). Fahrwerkhandbuch (738 p.). Vieweg+Teubner Verlag, Springer Fachmedien Wiesbaden GmbH.
29. Blundell, M., & Harty, D. (2004). The multibody systems approach to vehicle dynamics. Elsevier.